II International Conference on Particle-based Methods - Fundamentals and Applications
PARTICLES 2011
E. Oñate and D.R.J. Owen (Eds)

CALIBRATION OF PARTICLE-BASED MODELS USING CELLS WITH PERIODIC BOUNDARY CONDITIONS

JAN STRÁNSKÝ*, MILAN JIRÁSEK†

* Czech Technical University in Prague
Faculty of Civil Engineering
Department of Mechanics
Thákurova 7, 166 29 Prague 6, Czech Republic
e-mail: Jan.Stransky.1@fsv.cvut.cz

† Czech Technical University in Prague
Faculty of Civil Engineering
Department of Mechanics
Thákurova 7, 166 29 Prague 6, Czech Republic
e-mail: Milan.Jirasek@fsv.cvut.cz

Key words: Particle models, calibration, periodic boundary conditions, multi-axial loading, failure envelope

Abstract.

In this contribution, a systematic approach to the calibration of particle models, i.e. characterizing a relationship between microscopic (defined on the level of individual inter-particle bonds) and macroscopic parameters is presented. The procedure is based on simulations of basic cells with periodic boundary conditions (PBC). Firstly, a calibration for elastic properties is explained. A very good agreement between the results of static FEM simulations, quasi-static DEM simulations and theoretical formulas motivated by the microplane theory is found.

Then, basic ideas of calibration of inelastic parameters using PBC are explained on the simple case of uniaxial tension. The dependence of the results on the periodic cell orientation with respect to the localized process zone (that typically occurs in the post-peak range) is studied and the influence of the particle and cell size is covered as well. The gained knowledge is then applied in simulations of material failure under uniaxial compression and multiaxial loading. To demonstrate the applicability of the described method, the plane stress failure envelope for the investigated model is constructed for different combinations of microscopic parameters.

1 INTRODUCTION

Particle-based (or discrete) methods (for example the discrete element method - DEM) are modern tools for numerical simulations, which can be used across many engineering and scientific branches and often beat the most widely used numerical approach – the finite element method (FEM). The discrete methods were originally developed for soil mechanics [1], but nowadays their applications cover structural mechanics [2], fracture analyses [3], impact analyses [4] etc.

In DEM, the studied problem is discretized by discrete elements (e.g. particles), which are mutually connected by deformable bonds. "Microscopic" constitutive parameters of these bonds (e.g. stiffness, strength etc.) influence the behavior of the whole model on the macroscopic scale and the choice of a proper constitutive law and of values of micro-parameters play the key role in the resulting model quality. The micro-parameters are usually identified (calibrated) using some kind of optimization (from the easiest trial-and-error method to sophisticated sensitivity analysis [5]) such that the macroscopic behavior of the model corresponds to the actual behavior (e.g. to the experimentally observed one) as closely as possible.

The topic of DEM calibration was studied by many authors [5, 6, 7, 8], but only a few of them used periodic boundary conditions [9] and, according to our knowledge, there is no study of PBC in combination with post-peak behavior and strain localization. Results of elastic homogenization with PBC lie between bounds evaluated from kinematic and static boundary conditions. In inelastic calibration, using PBC can reduce (unreal) local stress concentrations when applying prescribed displacement or force on certain particles.

In section 2 the chosen particle model is described. Note that the proposed calibration method is applicable to any kind of discrete model. The PBC in context of both DEM and FEM are presented in section 3. Section 4 describes calibration of elastic and inelastic parameters. The effect of mutual orientation of load and periodic cell (causing the direction of strain localization zone in post-peak range) is demonstrated on a simple case of uniaxial tension and observed facts are used and verified on other loading cases. The results are presented in section 5. To demonstrate the applicability of the described method, the plane stress failure envelope for the investigated model is constructed for different combinations of microscopic parameters.

For DEM simulation we used the open-source software YADE [10] and for FEM simulation the open-source software OOFEM [11].

2 INVESTIGATED PARTICLE MODEL

The model used for calibration in this contribution consists of rigid spherical particles with uniform radius r. The initial spheres packing is random close created in YADE with dynamic compaction followed by relaxation. Figure 1 shows a very good quality of such packings in terms of packing fraction and bond direction distribution.

Initially, particles whose center distance l is less than $2rI_r$ (where I_r is the so-called

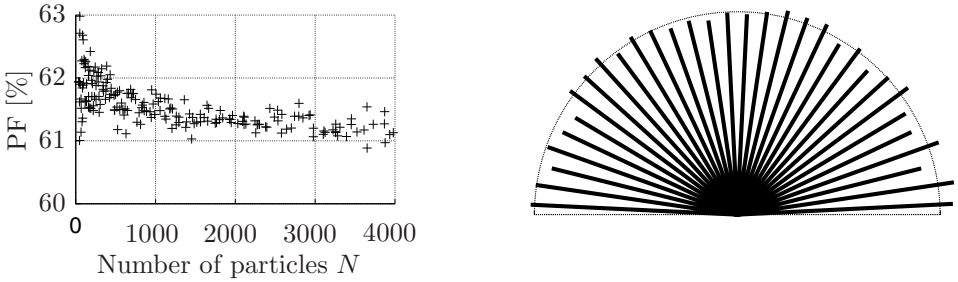

(a) (b)

Figure 1: Properties of random close packings: packing fraction for different number of particles (a) and bonds direction distribution for packing with 2278 particles and 16582 bonds (b).

interaction ratio) are connected. Each particle has 6 degrees of freedom (DOFs) – three displacements and three rotations. Each bond is characterized by its length l, unit normal vector $\mathbf{n}$, cross-section area $A = \pi r^2$ and internal forces $\mathbf{f}$.

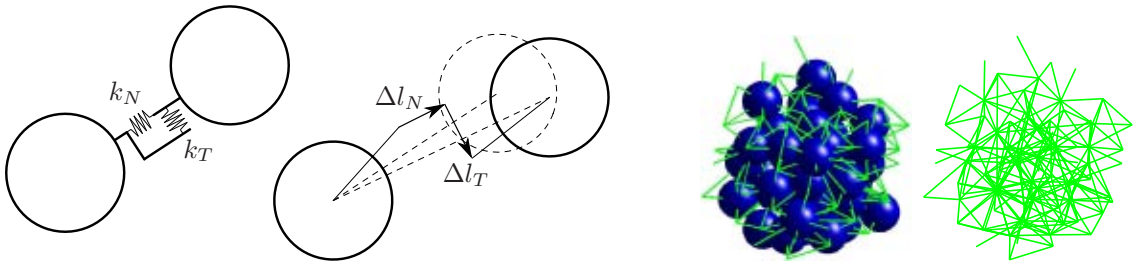

(a) (b) (c) (d)

Figure 2: 2D representation of bond elastic stiffness (a) and bond displacement (b), and example of particle assembly (c) and and bond network (d).

Bonds in our model have normal and shear (or transversal) elastic fictitious material stiffness E_b and G_b [Pa] and normal and shear bond stiffness $k_N = E_b A/l$ and $k_T = G_b A/l$ [N/m] (see fig. 2). In tension we used a bilinear damage mechanics law and in shear a Mohr-Coulomb-like plastic model (see fig. 3). Our simple model has 6 parameters that need to be calibrated, see table 1.

3 PERIODIC BOUNDARY CONDITIONS

Consider a periodic cell as a block filled with a periodic assembly of particles and bonds. Periodicity means that this cell (as well as all its particles and bonds and all their properties – velocity, stress, damage etc.) is surrounded by identical cells shifted along the cell edges, see fig. 4. For both studied methods (static FEM and dynamic DEM) there are special procedures how to incorporate PBC.

Table 1: Model parameters.

Symbol	Description	Units
E_b	Bond fictitious material normal stiffness	Pa
G_b	Bond fictitious material shear stiffness	Pa
ε_0	Limit elastic tensile strain	-
ε_f	Tensile strain when the bond is fully broken	-
c_0	Initial shear bond cohesion	Pa
φ	Bond internal friction angle	rad

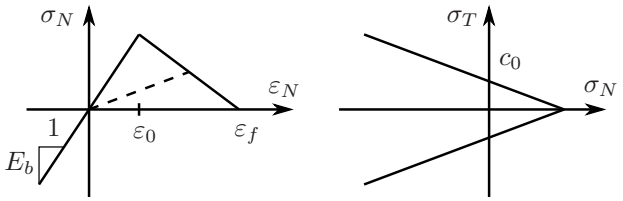

Figure 3: Considered constitutive law.

3.1 Static FEM solution

The linear part of the described model (including PBC) has been implemented into OOFEM with special nodes representing particles and special finite elements representing bonds. Each particle P has a displacement vector $\mathbf{u}_P$. Merging the displacement vectors of connected particles, a bond (element) displacement vector $\mathbf{u}$ is constructed and the element strain $\boldsymbol{\varepsilon}$ can be computed as

$$\boldsymbol{\varepsilon} = \mathbf{B}\mathbf{u}, \tag{1}$$

where $\mathbf{B}$ is element geometric (strain-displacement) matrix. In general, the element stiffness matrix $\mathbf{K}^e$ is defined in terms of $\mathbf{B}$ and material stiffness matrix $\mathbf{D}$ as

$$\mathbf{K}^e = \frac{1}{l}\mathbf{B}^\mathsf{T}\mathbf{D}\mathbf{B}. \tag{2}$$

The global stiffness matrix is assembled from particular stiffness matrices of all elements. The implementation of the PBC is analogous to [3]. Consider an element connecting one particle inside the cell with another particle physically located in one of the neighboring cells ($J'K$ and its periodic image JK' in fig. 4). PBC are imposed by the set of constraint equations that contain the components of macroscopic deformation $\mathbf{E} = \{E_x, E_y, E_z, E_{yz}, E_{zx}, E_{xy}\}^\mathsf{T}$. For instance, for link JK' and for x components we write

$$u_{K'} = u_K + E_x k_x C + E_{xy} k_y C, \qquad \phi_{xK'} = \phi_{xK}. \tag{3}$$

C is the dimension of the cubic periodic cell, constants k have values -1, 0 or 1 and specify the position of the particle outside the cell according to the relation (again only

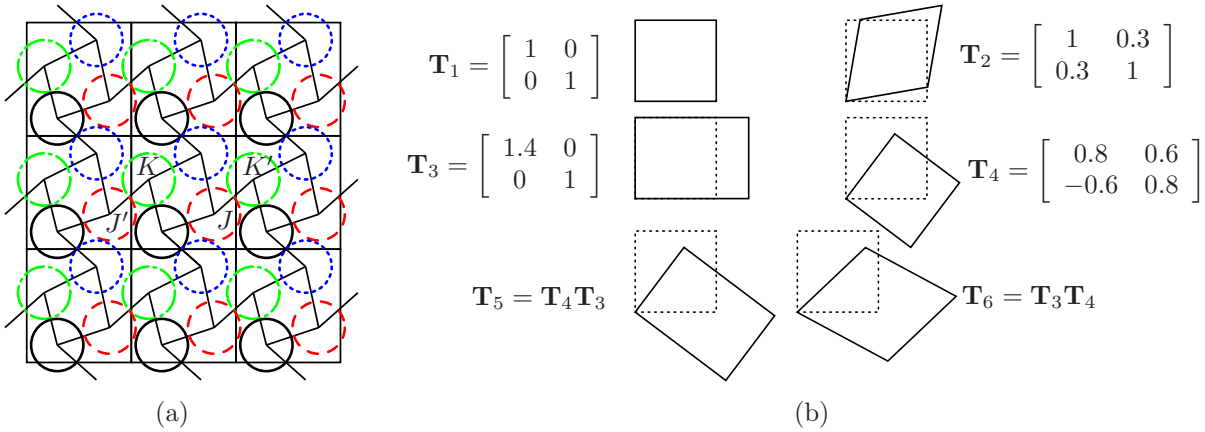

(a) (b)

Figure 4: 2D representation of periodic cells (a) and 2D representation of cell transformation (b).

for x direction)

$$x_{K'} = x_K + k_x C. \tag{4}$$

Using equations (3) and (4), the displacement of connected particles K and J' (periodic image of particle J) can be written in terms of the displacements of particles J and K and the macro-deformation $\mathbf{E}$ as

$$\left\{ \begin{array}{c} \mathbf{u}_K \\ \mathbf{u}_{J'} \end{array} \right\} = \mathbf{P} \left\{ \begin{array}{c} \mathbf{u}_K \\ \mathbf{u}_J \\ \mathbf{E} \end{array} \right\}. \tag{5}$$

Using the periodic transformation matrix $\mathbf{P}$, the modified stiffness matrix of the "periodic" elements can be expressed in the form

$$\mathbf{K}^e = \frac{1}{l}\mathbf{P}^\mathsf{T}\mathbf{B}^\mathsf{T}\mathbf{D}\mathbf{B}\mathbf{P}. \tag{6}$$

The components of macro-deformation $\mathbf{E}$ are therefore considered as global degrees of freedom. The corresponding "load" components are directly related to the macro-stress (they are equal to the stress components multiplied by the volume of the cell). To prevent displacement of the assembly as a rigid body, one particle needs to be "supported" by setting its three displacements to zero.

3.2 Dynamic DEM solution

The PBC for DEM are implemented in YADE. The periodic simulation is governed by the shape of periodic cell. We can modify the periodic cell via its 3x3 transformation matrix $\mathbf{T}$ (identity matrix initially) in two basic ways: rotation (when no strain occurs) and deformation (normal or shear strain without rotation), see fig. 4. At the beginning of our simulation, the cell is rotated to the requested position. The computational procedure

in a generic k-th step of simulation is as follows: First, the polar decomposition [12]

$$\mathbf{T}_k = \mathbf{U}\mathbf{H} \tag{7}$$

is performed on $\mathbf{T}$. $\mathbf{U}$ is an orthogonal matrix and $\mathbf{H}$ is a positive semi-definite symmetric matrix. Apart from this mathematical definition, polar decomposition has a straightforward geometric meaning: $\mathbf{U}$ represents rigid body rotation and $\mathbf{H}$ is related to the shape change. In terms of infinitesimal strain theory, the strain $\mathbf{E}$ is obtained as

$$\mathbf{E} = \mathbf{T} - \mathbf{I}, \tag{8}$$

where $\mathbf{I}$ is the identity matrix. Another definition of strain (e.g. logarithmic) could be incorporated.

The prescribed strain increment (in global coordinates) $\Delta\mathbf{E}$ is then appropriately rotated to cell's local coordinates and added to the shape matrix $\mathbf{H}$. Afterwards, the new value of $\mathbf{T}$ is composed from $\mathbf{U}$ and new $\mathbf{H}$:

$$\mathbf{T}_k = \mathbf{U}\mathbf{H}, \qquad \mathbf{T}_{k+1} = \mathbf{U}\left(\mathbf{H} + \mathbf{U}^{\mathsf{T}}\Delta\mathbf{E}\mathbf{U}\right) \tag{9}$$

Prescribed strain components can be directly applied via the cell's shape change. However, stress cannot be prescribed directly. Therefore, we developed a special strain predictor, which considers the values of stress and strain in a few last steps and predicts the strain value for the next step such that the value of stress is as close as possible to the prescribed one, see [10] for more details. The stress is computed according to [13] as

$$\begin{aligned}
&\boldsymbol{\sigma} = \frac{1}{V}\sum_{b\in V} l[\mathbf{N}f_N + \mathbf{T}^{\mathsf{T}}\cdot\mathbf{f}_T], \quad \mathbf{N} = \mathbf{n}\otimes\mathbf{n}, \quad \mathbf{T}^{\mathsf{T}} = \mathbf{I}_{\mathrm{sym}}\cdot\mathbf{n} - \mathbf{n}\otimes\mathbf{n}\otimes\mathbf{n}\\
&\mathbf{T}^{\mathsf{T}}\cdot\mathbf{f}_T = \mathbf{I}_{\mathrm{sym}} : (\mathbf{n}\otimes\mathbf{f}_T) - \mathbf{n}\otimes\mathbf{n}\otimes\cancelto{0}{\mathbf{n}\cdot\mathbf{f}_T}\\
&\boldsymbol{\sigma} = \frac{1}{V}\sum_{b\in V} l\left[f_N\mathbf{n}\otimes\mathbf{n} + \frac{1}{2}(\mathbf{n}\otimes\mathbf{f}_T + \mathbf{f}_T\otimes\mathbf{n})\right]
\end{aligned} \tag{10}$$

V is the cell volume, $\mathbf{n}$ is the bond unit normal vector, f_N and $\mathbf{f}_T$ are the normal and shear internal forces ($\mathbf{n}$ and $\mathbf{f}_T$ are perpendicular, therefore $\mathbf{n}\cdot\mathbf{f}_T = 0$), $\mathbf{N}$ and $\mathbf{T}$ are projection tensors and $\mathbf{I}_{\mathrm{sym}}$ is the fourth-order symmetric unit tensor. The sum is performed over all bonds b of the cell.

4 CALIBRATION

4.1 Elastic parameters

To obtain elastic macro-parameters numerically, from the structural response to a prescribed boundary displacement (under this constraint the elastic potential energy is not minimal and the response is stiffer than the real one) or to a prescribed boundary

force load (under this constraint the complementary elastic energy is not minimal and the response is softer than the real one), we can estimate the upper and lower stiffness bounds, respectively. PBC are a compromise between these two bounds and in general leads to better results [9].

A column of the macroscopic elastic stiffness (or compliance) matrix is equal to the macroscopic stress (or strain) caused by macroscopic strain (or stress) with unit value of investigated component and zero values of all other components. This method was used for both FEM and DEM simulations.

Theoretical analytical solution presented in [13] derived from prescribed macroscopic uniform deformation yields an upper bound estimation of elastic stiffness tensor

$$\mathbf{D} = \frac{1}{V} \sum_{b \in V} AL \left(E_b \mathbf{N} \otimes \mathbf{N} + G_b \mathbf{T}^{\mathsf{T}} \cdot \mathbf{T} \right) \tag{11}$$

$$D_{ijkl} = \frac{1}{V} \sum_{b \in V} AL \left[(E_b - G_b)\, n_i n_j n_k n_l + \frac{1}{4} \left(n_i n_l \delta_{jk} + n_i n_k \delta_{jl} + n_j n_l \delta_{ik} + n_j n_k \delta_{il} \right) \right] \tag{12}$$

Under the assumption of uniform probability of bond direction distribution, the following estimates of elastic constants (Young's modulus E and Poisson's ratio ν) can be derived (see [13] for more details):

$$E = E_b \frac{\sum_{b \in V} AL}{V} \, \frac{2 + 3\frac{G_b}{E_b}}{4 + \frac{G_b}{E_b}}, \quad \nu = \frac{E_b - G_b}{4E_b + G_b} \tag{13}$$

4.2 Inelastic parameters

PBC are also useful for calibration of inelastic parameters, usually ultimate stress/strain and shape of stress-strain (or force-displacement) diagram under specific load conditions (typically uniaxial tension or compression). For the case of uniaxial tension, a problem can arise when applying prescribed stress/strain on opposite "faces" of a specimen. If the sphere packing of the face is regular, the transition of regular to irregular (random) particle structure is usually broken and damaged first, before the "real structure" can be investigated. Another possibility would be to cut a plane from random packing and fix some particles up to a given distance from the face, but this can lead to stress concentration at the transition of fixed and unfixed particles and devaluation of simulation results. For this reason, the periodic boundary conditions seem to be suitable solution.

However, all that glitters is not gold. In the calibration with the help of PBC, we have to pay attention to the cell orientation with respect to the load, especially if strain localization occurs. In general, there exists an "optimal" orientation of the periodic cell, where the localized zone is parallel to the cell surface or is crossing the cell from one corner to another. For the simple case of uniaxial tension, the optimal orientation is zero. Then the localization zone (crack) has the minimal area (and is only one) and the minimal amount of energy is needed to split the cell. For other orientations, the periodic boundary

conditions force the crack crossing the cell boundary to continue at the periodic image of the cross point on another cell edge (see fig. 5). The crack is then longer than in the ideal case, more energy is needed for its propagation and the behavior of the cell is more ductile (see fig. 8). Notice the same behavior in pre-peak (elastic) range and different behaviors in post-peak (inelastic) range. The most ductile response is exhibited by a cell rotated by about 30°, the most fragile (as expected) by an unrotated cell. Results for 45° lie in between, see fig. 5 for illustrative example.

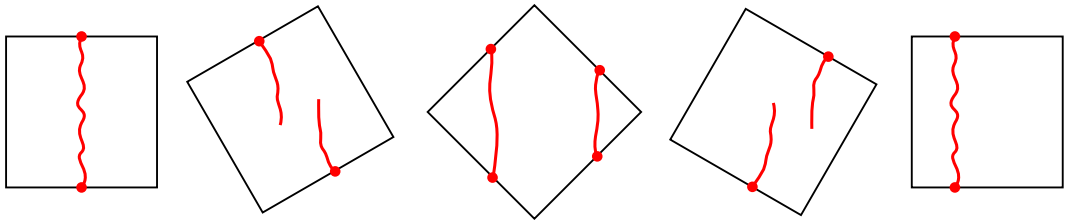

Figure 5: Different localization zone using PBC for uniaxial tension in horizontal direction

In a general calibration procedure, the most brittle (optimal) cell position has to be found numerically and its behavior is considered as the real one (unaffected by periodic boundary conditions).

5 RESULTS

The results of elastic calibration are summarized in figures 6 and 7, showing numerical and analytical values of Young's modulus E and Poisson's ratio ν for different interaction ratios. The numerical results of static FEM and quasi-static DEM simulations are indistinguishable from each other. The same fact can be observed for the analytical solution according to equations (11) and (13). For higher interaction ratios, the agreement between analytical and numerical solution is better and the analytical solution was verified to be the upper stiffness bound.

The elastic numerical simulations also verified that for a sufficient number of particles the model with random close packing is macroscopically isotropic and the results are rotationally invariant (the deviations get smaller for a higher number of used particles). The elastic results are size-independent.

For the inelastic part of calibration, we firstly verified our strain predictor, then the "quasi-staticity" of simulations and finally the post-peak results dependency on the cell orientation, see fig. 8. For the case of uniaxial tension, the most brittle ("optimal") behavior is obtained for a non-rotated cell.

Since the model exhibits strain localization, we can expect size effect phenomena. Similarly to pathological mesh size dependence in FEM, when the cell is cracked, the strain is localized into one layer of "elements" (bonds), while the rest of the cell is being unloaded. For a larger cell, the width of the localized area is relatively smaller and

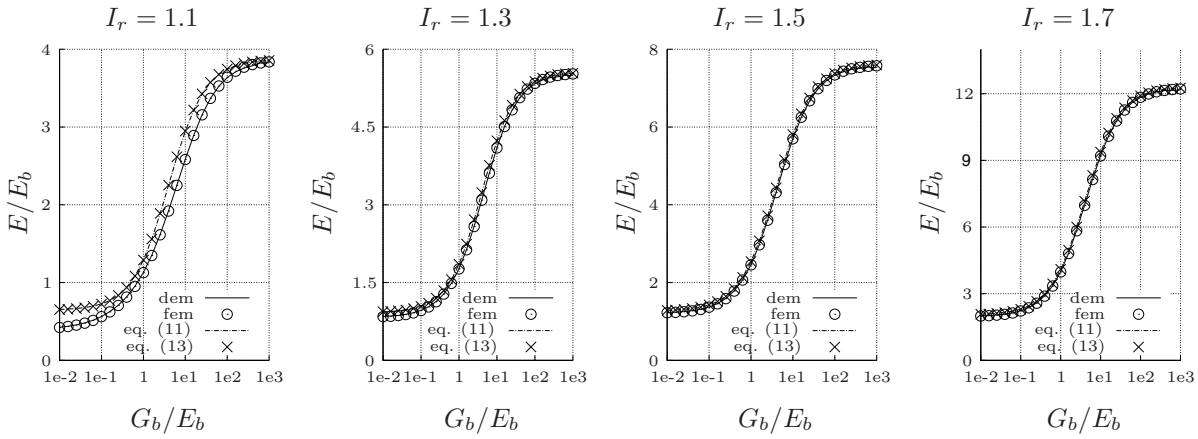

Figure 6: Ratio of macroscopic and bond Young's moduli E/E_b as a function of G_b/E_b ratio.

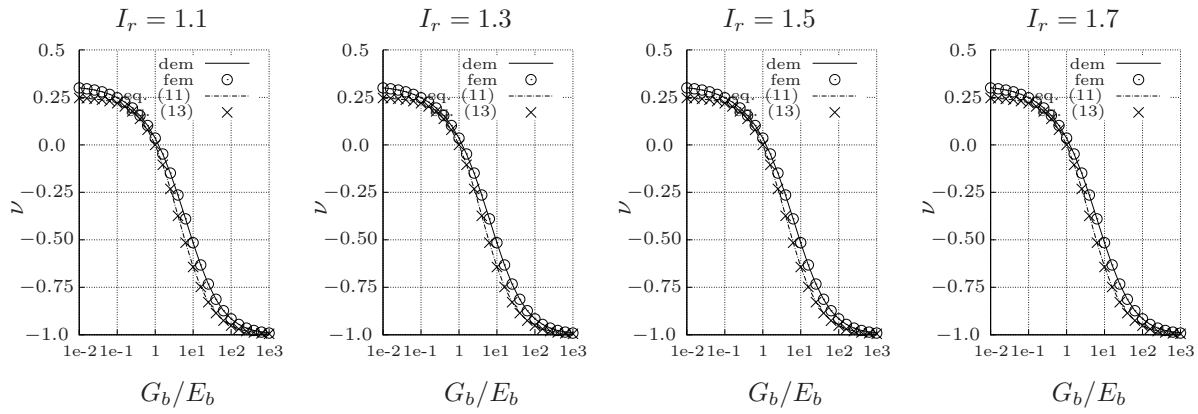

Figure 7: Poisson's ratio ν as a function of G_b/E_b ratio.

the resulting post-peak behavior is more brittle. This is shown in fig. 9 (almost no influence of the cell size on the elastic branch of the diagram and on the strength, but a significant influence on the post-peak behavior). Thus the microscopic parameters should be calibrated with respect to both particle (r) and cell (C) size. As seen in fig. 9, the results are influenced by the relative size of particles with respect to the cell size rather than by the absolute particle size.

For the case of uniaxial compression, the most fragile behavior occurs approximately for a rotation between 20° and 30° and for simple shear near 45°.

An important fact for all the studied cases is that the pre-peak (elastic) response is the same for all orientations (verifying isotropy of the model) and the strength (maximum reached stress) is also almost identical for all cases. Under this assumption, the plane stress failure envelope is constructed for different material parameters in fig. 10.

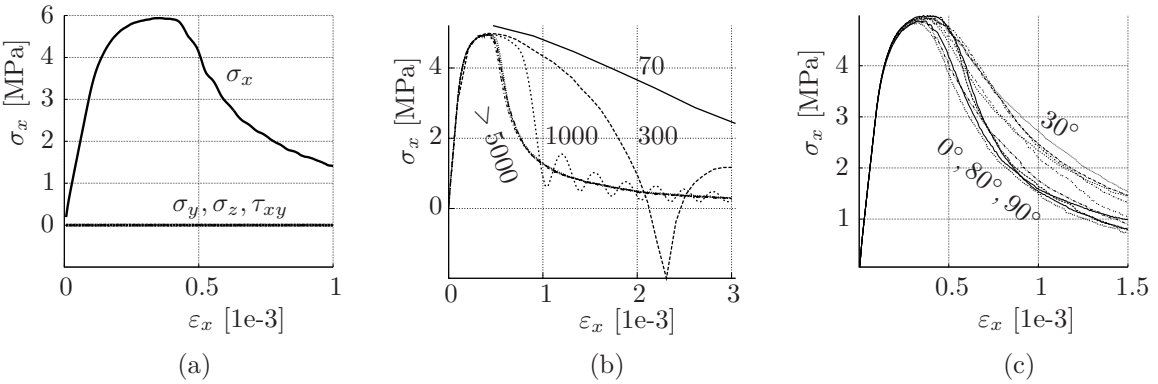

Figure 8: Verification of strain predictor (a), "quasi-staticity" (results are for constant final strain and different number of time steps) (b) and results dependency on cell orientation under uniaxial tension (c).

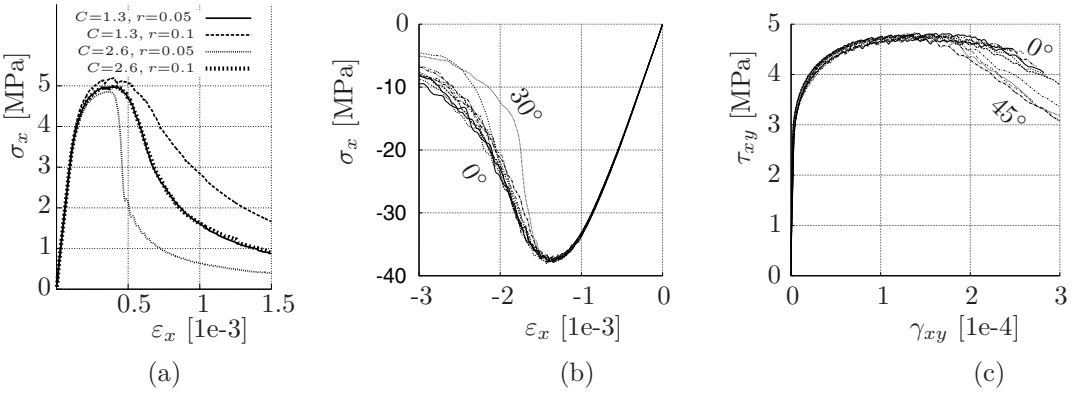

Figure 9: Results for uniaxial tension with different particle and cell sizes (a), uniaxial compression (b) and simple shear (c).

6 CONCLUSION

A systematic calibration method for discrete models with the help of periodic boundary conditions was presented. This method is applicable to any type of particle model and for both elastic and inelastic material parameters identification. The periodic boundary conditions have a positive influence on the results in the elastic range (it is a compromise between kinematic and static conditions).

In the case of inelastic calibration, PBC can reduce local stresses due to force or displacement prescribed on certain particles. A special attention has to be paid to the cell orientation with respect to the load. For realistic results, the optimal orientation (without negative effects of PBC) has to be found and the parameters should be calibrated on such an orientation. This orientation is parameter-dependent, so by changing the parameters to be optimized, the optimal calibration orientation can be changed as well.

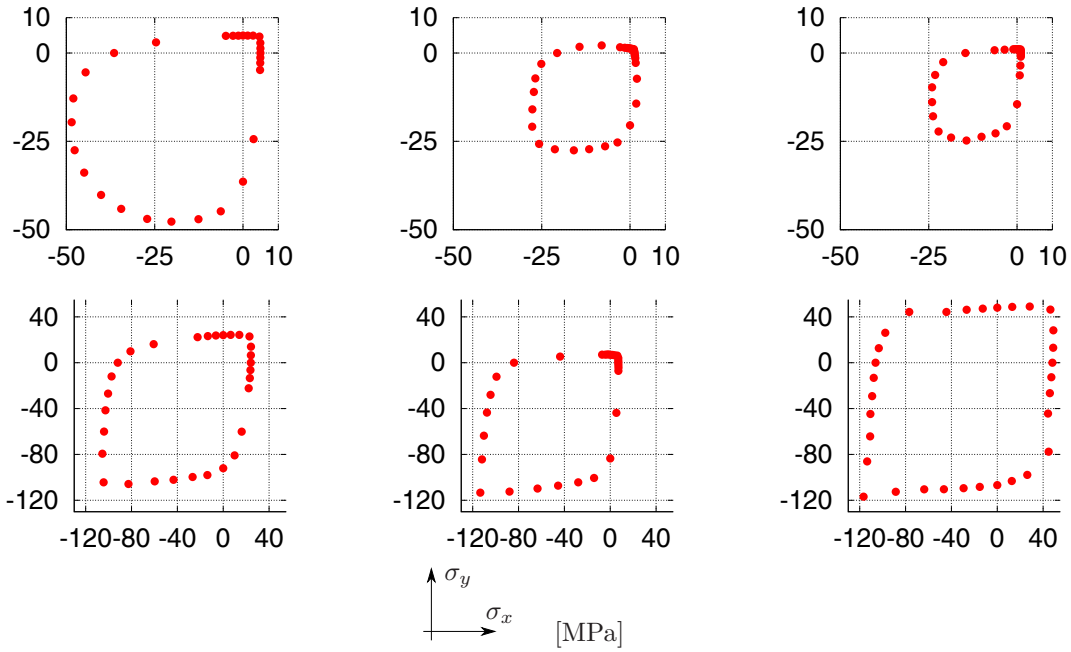

Figure 10: Figures of plane stress failure envelopes for different material parameters.

7 ACKNOWLEDGEMENT

Financial support of of the Czech Technical University in Prague under project SGS11/021/OHK1/1T/11 is gratefully acknowledged.

REFERENCES

[1] Cundall, P. and Strack, O. A discrete numerical model for granular assemblies. *Géotechnique* (1979) **29**:47–65.

[2] Pekau, O. A. and Yuzhu, C. Failure analysis of fractured dams during earthquakes by DEM. *Eng. Struct.* (2004) **26**:1483–1502.

[3] Grassl, P. and Jirásek, M. Meso-scale approach to modelling the fracture process zone of concrete subjected to uniaxial tension. *Int. J. Solids Struct.* (2010) **47**:957–968.

[4] Rousseau, J., Frangin, E., Marin, P and Daudeville, L. Multidomain finite and discrete elements method for impact analysis of a concrete structure. *Eng. Struct.* (2009) **31**:2735–2743.

[5] Wang, Y. N. and Tono, F. Calibration of a discrete element model for intact rock up to its peak strength. *Int. J. Numer. Anal. Methods Geomech.* (2010) **34**:447–469.

[6] Cotzee, C. J. and Els, D. N. J. Calibration of discrete element parameters and the modelling of silo discharge and bucket filling. *Comput. Electron. Agric.* (2009) **65**:198–212.

[7] Grima, A. P. and Wypych, P. W. Development and validation of calibration methods for discrete element modelling. *Granular Matter* (2011) **13**:127–132.

[8] Wang, Y. and Mora, P. Macroscopic elastic properties of regular lattices. *J. Mech. Phys. Solids* (2008) **56**:3459–3474.

[9] Miehe, C., Dettmar, J. and Zäh, D. Homogenization and two-scale simulations of granular materials for different microstructural constraints. *Int. J. Numer. Methods Eng.* (2010) **83**:1206–1236.

[10] Šmilauer, V., Catalano, E., Chareyre, B., Dorofeenko, S., Duriez, J., Gladky, A., Kozicki, J., Modenese, C., Scholtès, L., Sibille, L., Stránský, J. and Thoeni, K. *Yade Documentation*. The Yade Project, 1st ed., (2010), http://yade-dem.org/doc/.

[11] Patzák, B. and Bittnar, Z. Design of object oriented finite element code. *Adv. Eng. Software*. (2001):759–767.

[12] Computing the polar decomposition - with applications. *Siam J. Sci. Stat. Comput.* (1986):1160–1174.

[13] Kuhl, E., D'Addetta, G. A., Leukart, M. and Ramm, E. Microplane modelling and particle modelling of cohesive-frictional materials. In *Continuous and Discontinuous Modelling of Cohesive-Frictional Materials*, ed. P. A. Veemer et al. Springer, Berlin, (2001):31–46.